Int. J. Multiphase Flow Vol. 13, No. 1, pp. 33–46, 1987
Printed in Great Britain.

0301-9322/87 $3.00 + 0.00

THE MECHANISM OF VIOLENT CONDENSATION SHOCKS

G. CLASS, S. RAFF and R. MEYDER
Institut für Reaktorentwicklung, Kernforschungszentrum Karlsruhe GmbH, Postfach 3640, 7500 Karlsruhe, B.R.D.

(*Received* 16 *August* 1985; *in revised form* 15 *April* 1986)

Abstract—In direct-contact steam condensers, violent condensation shocks (VCSs) occur at low steam flow rates. This phenomenon was also observed in the pressure-suppression system of nuclear boiling water reactors. Thus, the phenomenology of condensation in this type of condenser has been investigated. The main design feature of the Plexiglas test apparatus used here is that the events of rapid steam–water condensation are observed in a sectional view instead of an external view. This allows the phenomena at the phase interfaces to be observed in detail. In our experiments we found that a characteristic feature of VCSs is the appearance of considerable entrainment inside so-called steam pockets, which is characterized by atomization and is correlated to the extremely high rate of condensation. This avalanche-like increase in water atomization is induced by the Kelvin–Helmholtz instability and occurs because of the increasing steam flow velocity along the freely movable surface of water, primarily in the bottle-neck of the steam pocket. Detailed examination of the experimental data shows that the entrainment causes the temporary high condensation rates, which were previously observed but not understood. This is in agreement with the conditions of a sonic steam jet blowing into a subcooled pool of water where entrainment stimulates the condensation process in a similar way. The extraordinarily high condensation rates in the steam pocket induce very high steam velocities in the vent pipe, so that the entrainment often propagates outside the steam pocket in the vent pipe. We conclude that the initiating mechanism of VCSs is this self-amplifying feedback process which lasts until the initiating steam pocket has disappeared. The induced state of rapid condensation outside the steam pocket decays with a time constant in the range of 0.1 s.

1. INTRODUCTION

During the direct condensation of vapour vented into a pool of cold fluid, violent condensation shocks may occur. These shocks cause considerable mechanical loads on the structures. Knowledge of the mechanisms of direct condensation is therefore of interest for the operation of plants in the chemical process industry, cf. Bouré *et al.* (1973), as well as for the pressure-suppression system (PSS) of boiling water reactors (BWRs), cf. Bankoff (1980).

In the case of steam vented through a pipe into a pool of cold water, the phenomenon of rough condensation at low steam flow rates is called chugging, cf. Marks & Anden (1979). After formation of a steam bubble at the lower end of the submerged condensation pipe, the condensation rate increases rapidly, causing low steam pressure in the pipe. This forces the water into the pipe, where the condensation rate falls to much lower values. As a result the steam pressure increases and the water is pushed out of the pipe again. A new bubble will then be formed, and so on.

The condensation process varies in detail from event to event. The peaks in the condensation rate occur rather randomly. Sometimes the steam pressure is decreased quite abruptly. This indicates, that the condensation rate can increase suddenly and very rapidly. Such a condensation event is termed a "violent condensation event" or preferably a "violent condensation shock" (VCS) in the following. This term suggests that the most violent condensation events are associated with shock-type flow conditions in the steam and also by shock-type mechanical loads on the structures.

To date, it is not clear which physical processes caused these VCSs. Experimental observations of bubbles collapsing at the outlet of condensation pipes, performed using high-speed cinematography (Marks & Anden 1979; Lee 1979; Aust & Sakkal 1981; Sonin 1981), have not given satisfactory insight into the dynamic behaviour of the steam–water interfaces. Published theoretical studies usually start using the classical models of bubble growth and bubble collapse with a description of flow conditions using a Rayleigh approach. With these models the condensation is driven by the heat transport from the smooth bubble surface through a layer of condensate into the colder fluid. However, evaluation of the existing experimental data reveals that in the case of shock-type condensation, the heat-transfer coefficient must be increased abruptly by about 2 orders

of magnitude [condensation burst, Bankoff (1980)]. This phenomenon could not be successfully interpreted in a physically convincing way (Sonin 1981).

Thus, the aim of the present investigation is to identify the basic mechanisms of shock-type condensation processes.

As the boundary conditions for the occurrence of such condensation shocks are well-known in the PSSs of BWRs (cf. Marks & Anden 1979; Lee 1979; Aust & Sakkal 1981; Sonin 1981; Class 1977), we performed an experimental investigation of these VCSs in a test facility similar to such PSSs. In PSSs of BWRs (e.g. version '69 of KWU, or MARK 2 of GE), the steam to be condensed is vented through vertical pipes (600 mm dia) into a pool of water. The pipes run 2–3 m down into the water. In preliminary experiments with water and air we found that a radially cut system arrangement (Class 1981) offers promising test and observation conditions. Instead of seeing only the three-dimensional bubble surface and its movement from "outside" we have a cut through the bubble and the wall of the pipe. Therefore, we can see the movement of the phase interface as well as the water and steam flow indicated by small bubbles or droplets, respectively. Such two-dimensional flows are much easier to interpret than three-dimensional ones; this is the reason why, for our condensation experiments, we used a Plexiglas model which represents a 30° sector of one pipe of a PSS.

2. TEST FACILITY AND INSTRUMENTATION

A reduction of the full-scale PSS at a scale of 1 : 3 has been considered to be justifiable in order to maintain the characteristic flow conditions of the condensation process. Figure 1 shows the

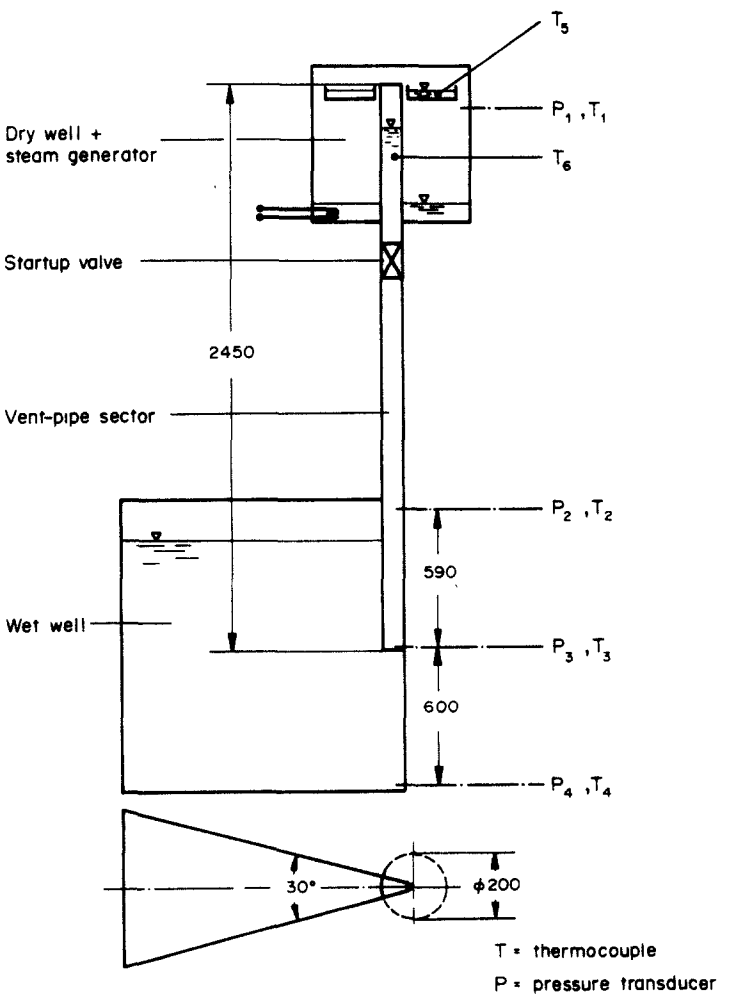

Figure 1. Outline of the test facility with the instrumentation.

turbulence, is then given. Finally, the generalized lubricating-film model predictions are compared with core-flow pressure gradients measured in the 5 cm test facility.
principal design features of our test facility which consists of a 30° sector of the pool containing a 30° sector of one condensation pipe. This arrangement allows good observation of the approximately two-dimensional flow conditions around the edge of the pipe, since cylindrical symmetry can be assumed. The vertical walls of the sector were made of Plexiglas sheets. As figure 1 shows, the apex of the wedge is cut off in order to avoid trapping of liquid. The influence of the additional wetted walls on the condensation effects was expected to be insignificant. The fact that only about 1% of the steam mass flow rate of a full-scale PSS has to be supplied to reach the range of VCSs is an advantage in performing the experiments.

The steam source and the reactor dry well are simulated by a steam tank containing a 5 kW electrically heated steam generator. The initial steam pressure at the start of an experiment was usually held at about 117 kPa. The amount of steam provided by this tank is increased by latent steam storage using 15 steel basins filled with water at saturation conditions (in figure 1 only one of these basins is shown). The basins are kept filled with boiling water during the experiment by a steam-water flow driven by natural convection.

With this design a mean steam mass flow rate of about 20 kg/m^2 s can be produced. For such test conditions, the data of Chan & Lee (1982) and Cumo *et al.* (1978) indicate a broad variety of modes of condensation.

Below the steam tank, a quick-opening valve is installed which has a double cone plug. In the closed condition the plug is held in the upper position by an electromagnet. When the electric current is switched off, the plug falls in the direction of the steam flow into a position providing the full flow area of the vent pipe. By means of this valve the condensation experiment can be started from well-defined initial conditions at a well-defined time.

Figure 2 shows the complete test facility with the Plexiglas pool. The lower segment of the pipe is made of steel for reasons of stability. Near the outlet of the pipe, exchangeable plates of Plexiglas have been installed on both sides of the sector. The plates are replaceable here because in this region the observation windows become increasingly marred by microcracks.

In the foreground two high-speed cameras are set up which record the events near the pipe outlet and inside the condensation pipe. The picture frequencies during recording were either 1000 or 3000 Hz. Transmitted and incident light were both used for filming with the former predominating.

Additionally, pressure and temperature have been measured at four elevations (cf. figure 1): in the steam reservoir, in the condensation pipe 590 mm above the pipe outlet, at the pipe outlet and at the bottom of the water pool 600 mm below the pipe outlet. For the temperature and pressure measurements, fast sheathed thermocouples (0.25 m dia) and miniature membrane-pressure transducers with strain gauges (Sensotec M530) were used, respectively.

Recording of the experimental data was done by a central data-processing system (Hymeda). The recording frequency was 2 kHz per data channel. All the data have been digitized on-line and stored. In order to have an exact time correlation between the experimental data and the films, the process time of the computer has been faded into the picture area of both cameras.

3. TEST PROCEDURE

The water column in the upper part of the condensation pipe is heated due to the integration of the pipe into the steam generator. Thus, the influence of a layer of hot water on the condensation process could be investigated. The following initial conditions have been used:

—the water column above the valve is at boiling temperature;
—the water column above the valve is cold;
—the volume above the valve is filled with steam.

The latter initial condition results in a cold water column with reduced potential energy.

The following test parameters have been kept constant:

—the temperature of the water pool was 25°C;
—the initial pressure in the steam reservoir was about 117 kPa;
—the depth of immersion of the condensation pipe into the pool was 400 mm.

Figure 2. General view of the test facility (the high-speed cameras are in the foreground).

After preparation of the water levels in the steam tank, the water level in the pipe is raised above the quick-opening valve by evacuation of the steam tank with the valve in the open position. Usually the pipe was filled totally with water prior to the start of the experiment to prevent impairment of the condensation process by non-condensible gases remaining in the upper part of the pipe. The valve is then closed the steam generator heated up until the water in the basins has reached boiling temperature due to steam condensation. Then the residual air in the steam tank is removed by repeated release of steam through a valve on top of the reservoir.

The experiment is initiated by the actuation of the quick-opening valve. At the same time data recording and the cameras are started.

4. THE OBSERVED CONDENSATION PROCESSES

As already mentioned, the steam used in our test facility is stored in a tank; which is why, in one experiment, usually four cycles of bubble formation and collapse can be observed. For each of these cycles the nominal steam flow rate is different. One cycle lasts about 1 s.

The total course of a typical experiment is outlined in figure 3 by means of the pressure and temperature signals at the pipe outlet and at a position 590 mm above the outlet. The thermocouples T_2 and T_3 indicate changes in the water level in the pipe. Minimum values correspond to the water temperature, and maximum values to the steam temperature. As can be seen, the steam volume reached the thermocouple T_3 four times. The pressure oscillations are consequences of

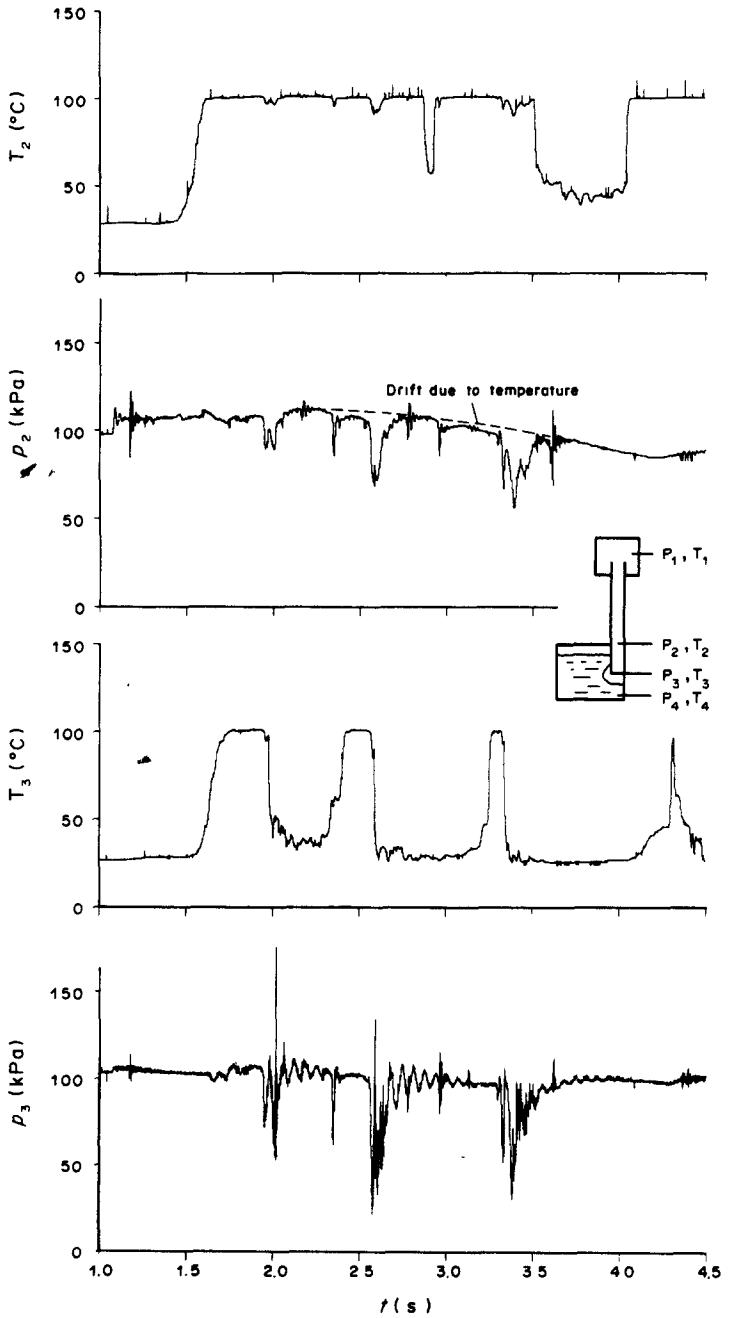

Figure 3. Temperature and pressure signals during an experiment.

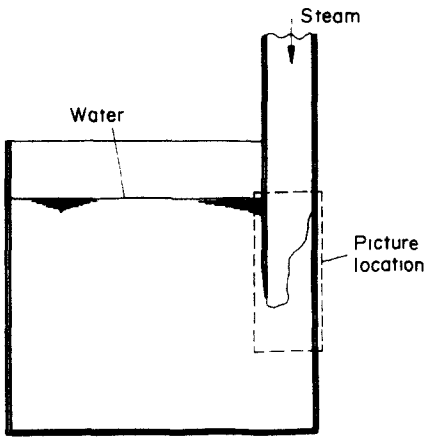

Figure 4. Location of the pictures taken with the cameras.

individual condensation shocks, which are described in the next section. Figure 3 shows clearly that in this experiment three strong and one weak chugging events are traced.

With the two high-speed cameras films have been taken of the VCSs. The films show the section indicated in figure 4. These films contain the main information about the condensation mechanisms in our experiments. But the presentation of this information proved to be impossible on the basis of only the single figures extracted from the films. The process of this highly dynamic VCS can only be recognized and physically interpreted by repeated visual study of the films. The main result of our work is the identification of typical initial configurations of phase interfaces which lead to a VCS. This identification or data reduction, similar to the recognition of patterns, was not possible without some interpretation. The simplified characteristic initial conditions we have identified in this way are shown schematically in figure 5, where axisymmetry was assumed. The types of events shown in figures 5a–g are arranged roughly chronologically with respect to the course of an experiment.

The VCS after initiation of a test at high steam flow rates is usually a jet-type VCS (a). After

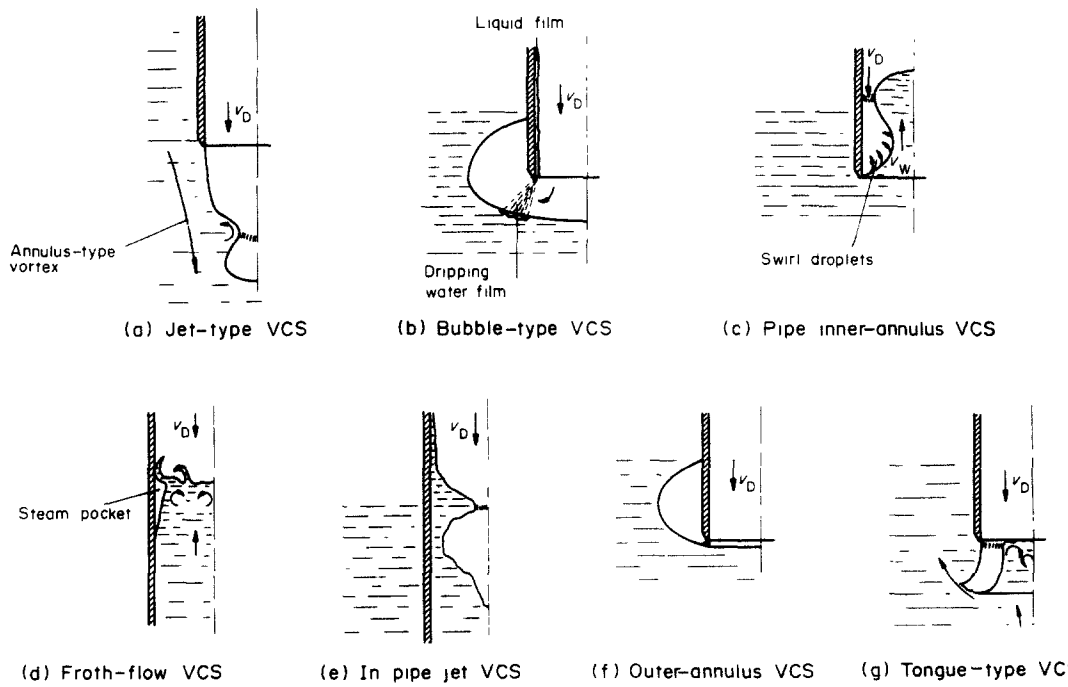

Figure 5a–g. Typical initial conditions prior to a VCS (main steam flow v_D).

decay of the steam jet or after a number of VCSs at lower steam flow rates we find a bubble-type VCS at the lower end of the condensation pipe (b).

After a VCS outside the condensation pipe, e.g. a bubble- or jet-type VCS, the water flows back into the pipe. During this period we find at the entrance of the pipe a recirculating flow or wake filled with steam. This wake would form a steam-filled annulus if the test rig were not a 30° section. This is a pipe inner-annulus VCS (c).

The pipe inner-annulus VCS causes a very turbulent froth flow of subcooled water inside the condensation pipe. In this flow steam can be encapsuled which, due to condensation in the "bubble", collapses and amplifies the froth flow again. This is a froth-flow VCS (d). Besides the jet-type VCS outside the condensation pipe (a), a jet-type VCS can also be identified inside the pipe (e).

With very low steam flow rates we find a pipe outer-annulus-type VCS (f) and a tongue-type VCS (g).

The configurations of the steam–water interface, as shown in figures 5a–g, exist for about 0.1 s. In all these cases there exists a zone of decreasing cross-section for steam flow, as indicated in figures 5a–g. Then in the films this zone was shading for each of the individual VCS types, the steam volume detached and the bubble collapsed within a few hundreds of a second. During detachment, with incident light, an increasingly darkening spot could be observed at the zones mentioned, which expanded rapidly over the whole steam area.

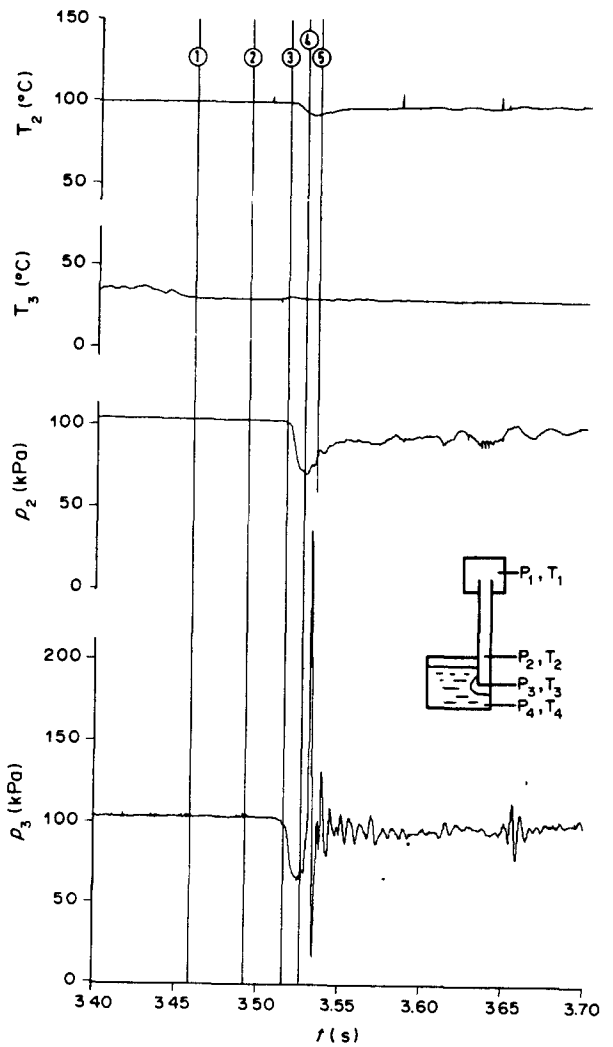

Figure 6a. Pressures and temperatures vs time of a pipe inner-annulus condensation shock.

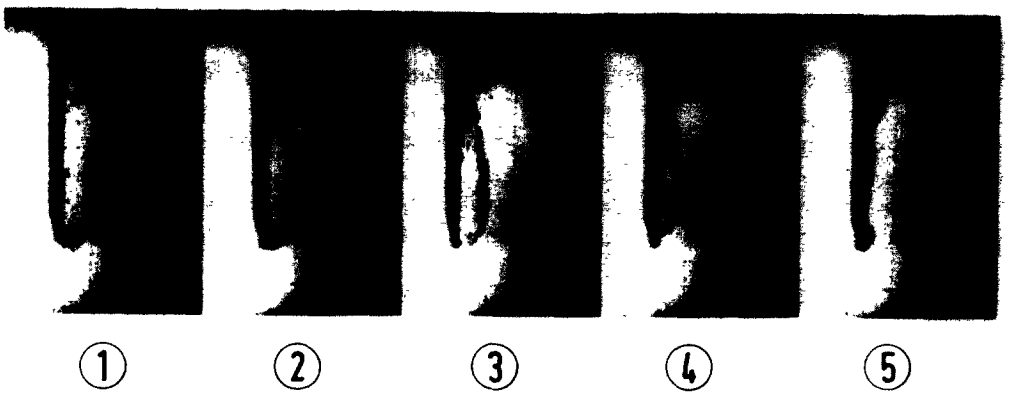

Figure 6b. Characteristic pictures of a pipe inner-annulus condensation shock (the numbers refer to the times of figure 6a).

As an example of the data recorded and the pictures taken during a test, figures 6a,b show the time-dependent data and pictures at five characteristic times for a pipe inner-annulus VCS. At time 1 the steam-filled wake at the pipe entrance is connected with the steam volume in the pipe. T_2 and p_2 reflect steam data at this time, and T_3 and p_3 reflect the corresponding data of the water. At time 2 the picture in figure 6b shows the beginning of the detachment of the steam wake (bubble). The location of the detachment becomes darker and darker. At time 3, when the detachment is almost complete, the pressure falls very rapidly, in the steam as well as in the water. Within 10 ms the pressure drops by 40 kPa. At time 4 the pressure minimum is reached and the bubble is detached. The dark zone in the pictures grows at an increasing rate and covers almost instantaneously the bubble and the steam in the upper part of the condensation pipe. After a delay of about 5 ms at time 5 the steam annulus has completely collapsed and the pressure shock occurs. In the figure cloudy water is seen due to very fine gas-containing bubbles at the locus of the collapsed steam annulus. As can be seen with p_2 and p_3, the frequency of the pressure oscillation is higher in the water than in the steam, due to the higher velocity of sound in the water pool. Along with the changes in the pressure p_2, we find also changes in the temperature T_2 in the steam. Thermocouple T_3 remains permanently in the water phase during this event because it is a pipe inner-annulus-type VCS.

5. THE MECHANISM OF VCSs

Since our main results are deduced from the films, we use them as a basis to formulate a hypothesis on the mechanism of a VCS. Subsequently, we check it by means of the temperature and pressure histories as well as with data deduced from them.

Figures 5a–g illustrate that the size and shape of the phase interface are determined by the steam pressure and inertia of the water. So the jet- and bubble-type VCSs, (a) and (b) respectively, reflect a higher steam pressure, whereas the outer-annulus and tongue-type VCSs, (f) and (g) respectively, reflect a lower one. The inertia of the water is evident for the pipe inner-annulus-type VCS, but it is also present for the jet- and bubble-type VCSs. This can be explained as follows: whenever water flows out of the condensation pipe, especially at the beginning of an experiment, an annulus-type vortex is formed in the pool, as indicated in figure 5a; consequently, the water in the pool flows down along the condensation pipe stretching the interface in the jet-type VCS and pressing the bubble down in the bubble-type VCS.

A further parameter characterizing the VCS types is the apparatus used. In our experiment the side walls of the 30° sector may have a slight influence on the VCS types (c)–(e). So if a different arrangement of the condensation pipe and water pool were used, additional VCS types might be observed. However, we found a common pattern for all our VCS types. There is a steam volume in the fluid which is connected to the steam source by a channel which has a considerably smaller and, with time, further decreasing cross-section than the steam volume itself. We term the steam

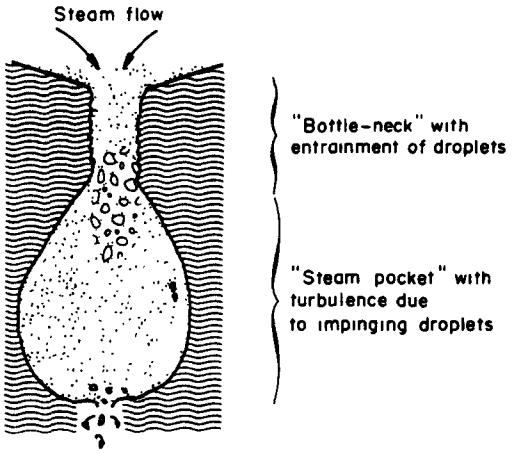

Figure 7. Basic characteristics of a steam pocket.

volume a "steam pocket" and the channel the "bottle-neck" of the pocket, A schematic representation of this characteristic pattern is given in figure 7.

The dynamics of a VCS are determined by the junction between the pocket and the steam source (figure 7). The analysis of the present experiments shows that the condensation rate in the pocket is strongly affected by the steam flow in this junction. During the formation of the pocket steam flows into the pocket through the bottle-neck. In the case of a pocket growing in size there is an increase in the interfacial area, and therefore an increase in the overall condensation rate, requiring an increased steam mass flow rate through the bottle-neck. At the same time, the bottle-neck cross-section is decreasing because of the inherently unstable configuration of the steam pocket. As a result, the steam velocity in the bottle-neck increases more and more rapidly. Due to the interaction between the accelerating steam flow and the water surface, surface waves are generated by Bernoulli forces. This effect can be interpreted as a Kelvin–Helmholtz instability (KHI). With the increase in steam velocity these surface waves will become shorter and, relative to the wavelength, more amplified. Above a certain critical velocity in the bottle-neck an avalanche-like growing entrainment of very fine atomized droplets occurs, leading abruptly to a strong increase in the liquid–vapour interfacial area and the related condensation rate. We term this self-amplifying feedback process "steam-pocket instability". This process lasts until the initiating steam pocket has disappeared.

With this understanding of the process we interpret the dark clouds, seen in the films in transmitted light, starting in the bottle-neck, spreading out downstream in the steam pocket and, due to the high steam velocity induced, often also upstream in the vent pipe, as swarms of entrained very fine droplets. This is in agreement with Catton *et al.* (1980), who proposed such an effect to interpret their results.

In the bottle-neck similar phenomena appear which are known from the gas flow over a horizontal liquid surface, i.e. an initial wave formation due to the KHI and finally the entrainment at higher flow velocities. The wavelengths and amplitudes here, however, may be very small. Following Langner (1978), the drops formed will be much below 0.1 mm at the high steam velocities observed here. These fine droplets can be seen in our experiment using incident light as dense clouds of white fog. In our case most of the two-phase interfaces are arranged vertically and the wave formation is controlled solely by capillary forces (surface tension). This is in contrast to the usual case with horizontal liquid surfaces, where the wave formation is controlled by both gravity and surface tension. As a consequence the KHI criterion gives no distinct critical velocity, i.e. every velocity causes growing wave amplitudes. Also, the highly transient character of the entrainment process discussed here may be responsible for the resulting avalanche-like atomizing process instead of the usual droplet entrainment.

In addition to the pressure drop in the pocket due to condensation, there is a pressure drop in the bottle-neck due to the higher steam velocity in the reduced cross-section. This effect can be interpreted as the longest occurring KHI wavelength. Thus, the low pressure in the bottle-neck

starts to detach the pocket as the surrounding fluid accelerates closing the bottle-neck. At this time, the pressure in the steam pocket can easily reach a level where the critical pressure ratio (sound velocity) along the bottle-neck is obtained. From the bottle-neck, a low-pressure wave then evolves and propagates at almost sound velocity within the condensation pipe, causing further entrainment at the wetted pipe wall. Finally, the bottle-neck is closed completely and the evacuated pocket collapses rapidly.

The occurrence of entrainment originating from the liquid films at the vent-pipe walls is a result of the low-pressure wave caused by the earlier "steam-pocket instability" and has no influence on this initiating mechanism. But the entrainment of the droplets and their redeposition on the free water surfaces enhance local water turbulence and amplify the condensation rates.

The condensation rate within the steam pocket is determined by both the condensation on the surface of entrained droplets and the condensation on the free surface of the steam pocket. For the latter, the surface temperature is controlled by the turbulence of the fluid providing heat transfer from the liquid surface to the bulk liquid. The entrained droplets, accelerated by the very fast steam inside the bottle-neck and the steam pocket, strike the two-phase interface at the pocket side walls and bottom at a high speed. The resulting swirl effect enhances the fluid turbulence and thus the condensation rate.

Thus we conclude that a self-amplifying entrainment process accompanied by an increased turbulence in the water boundary layer, originating from a steam-pocket instability and propagating into the vent pipe, are the reasons for the high condensation rates and the strong pressure reduction in the course of a VCS.

6. QUANTITATIVE EVALUATION OF THE EXPERIMENTS

Measurements of the most interesting variables like steam velocity, interfacial area or condensation rates are not directly available in our experiments. These quantities, however, are deduced as described in the following. We analyse primarily the VCS-type "pipe inner annulus" shown in figure 6b because it represents approximately a typical "deep-water steam pocket", and because of its larger size and larger time scale relative to most "deep-water steam pockets" observed in our experiments.

Figure 8a shows the pressure histories of p_1 and p_2 used for the determination of the steam velocity and the steam mass flow rate. In these data the global reduction of the pressure level of about 18 mb/s is neglected and corrections were made to compensate a temperature-induced drift for p_2.

Figure 8b shows the total effective interphase area and its portion in the steam pocket, as seen in the films. The interface was smoothed and the wetted side walls are not taken into account. The steam pocket is formed shortly before time 1. During the closure of the bottle-neck the steam pocket is decoupled from the steam generator, therefore the interphase area in the pocket is assumed to decrease linearly to zero between time 3 and 4.

To determine the steam velocity in the vent pipe shown in figure 8c a momentum-balance equation was solved for the gas flow between the locations of p_1 and p_2. In the balance, the pressure histories (cf. figure 8a), the vent-pipe cross-section and friction losses are used. The steam velocity in the bottle-neck, also given in figure 8c, is deduced from the vent-pipe velocity and the steam flow, taking into account the ratio of the interphase area in and outside of the steam pocket and the flow cross-sectional area in the bottle-neck, as seen in the films. According to figure 8c the steam velocity in the bottle-neck exceeds some 100 m/s before time 3.

For the determination of the condensation rate, shown in figure 8d, a mass-balance equation for the vent pipe was solved using the steam density and the steam velocity of figure 8c, allowing mass storage in the lower part of the vent pipe indicated by pressure p_2. The estimated condensation rate within the steam pocket is also given in figure 8d, based on the phenomena seen in the film between times 3 and 4. According to this, the condensation rate within the steam pocket shows a sharp increase at time 3 where the steam velocity in the bottle-neck has already exceeded some 100 m/s (cf. figure 8c). At time 4 the critical pressure drop for the steam flow in the bottle is probably reached.

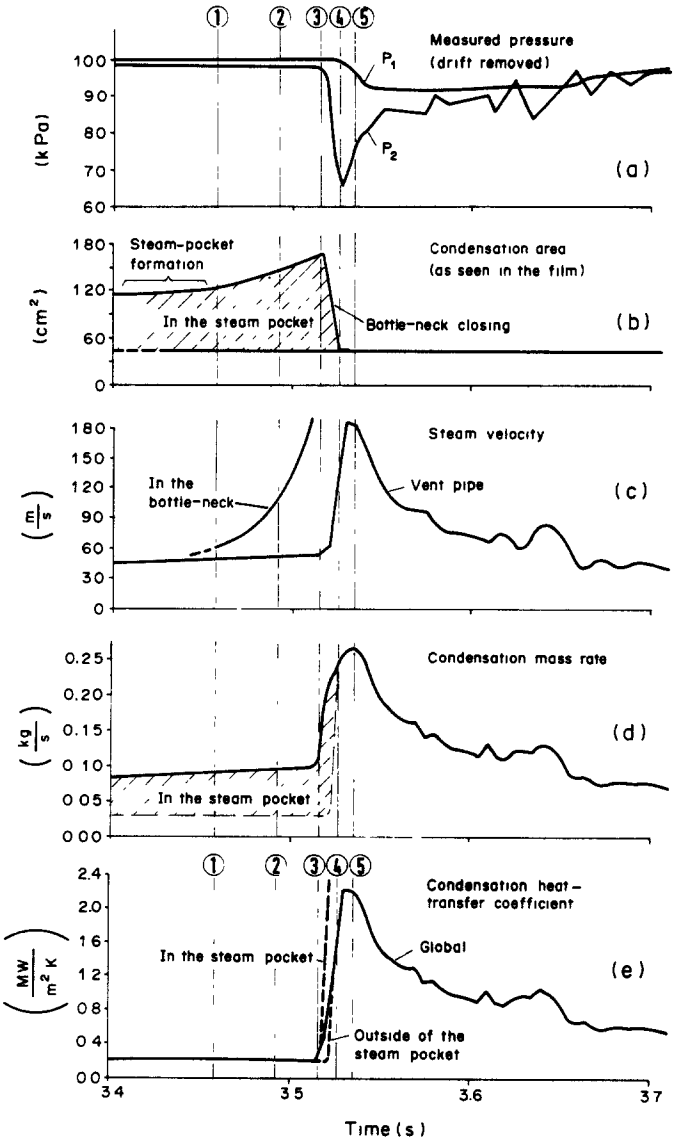

Figure 8a–e. Data for a pipe inner-annulus condensation event [(c)–(e) are inferred from the observations in (a) and (b), times 1–5 refer to those of figure 6b].

Figure 8e shows the heat-transfer coefficients, calculated as latent heat × condensation rate, normalized with the interphase area and the difference between steam saturation and bulk pool tempeature. Additionally, estimated curves are given for the heat transfer outside the steam pocket. The sharp increase in this coefficient after time 3 inside the steam pocket is due to the very efficient water atomization at critical steam flow.

In figures 8a–e we can see clearly a propagation effect. At first the entrainment in the bottle-neck (cf. figure 6b) leads at time 3 to a sharp increase in the global condensation rate and causes increased steam velocities in the vent pipe. The subsequent steam-pocket instability detaches the steam pocket and leads to a further increase in the steam velocity outside the steam pocket, so that at time 4 entrainment and increased turbulence in the water is found even there. That is why high condensation rates and heat-transfer coefficients are found for the pipe inner-annulus VCS even after the pocket has collapsed. The high condensation rates decay within 0.1 s.

A comparison of our heat-transfer coefficients with those of Catton *et al.* (1980) shows that for the pipe inner-annulus VCS a heat-transfer coefficient of about 0.2 $MW/m^2 K$ prior to time 3 is relative high. We assume that this is due to the high level of turbulence which is produced during

the flow of the water around the edge into the vent pipe. The condensation heat-transfer coefficients of the pipe inner-annulus VCS investigated here have values up to about 2.2 MW/m^2 K. They are in good agreement with the value of 1 MW/m^2 K found for the detached bubble collapse by Catton *et al.* (1980) and the value of 3.5 MW/m^2 K found for a sonic steam jet by Cumo *et al.* (1978). Cumo *et al.* identified basically the same heat-transfer mechanism for the sonic jet as we have found for the VCS, namely entrainment resulting from the two-phase interface instability in a gas flow parallel to the interface. In the case of a steam jet with the critical velocity however, the high steam velocity is maintained by the overpressure in the steam vessel in a steady-state mode. This is in contrast to the VCS, where the overpressure is low and the high steam velocity results from a transient, self-driven condensation process. The required pressure drop is created, given a suitable shape of the two-phase interface, by the escalating condensation and by the briefly and locally established sub-pressure in the steam pocket.

The question whether the latent heat of the steam during a VCS is primarily absorbed by the entrained droplets or in the turbulent liquid at the phase interface could not be completely clarified. The sequence of events according to figure 8a–e however leads to the conclusion that condensation at the dispersed fine droplets is dominant in the initial phase of a VCS. However the turbulence in the water seems to become important in two cases: (1) in the final phase of a VCS when the steam–water interface is in the vent pipe and the entrainment process has propagated outside the steam pocket; (2) with the encapsulating steam bubble, where only a relative thin water film at the pipe wall is available for entrainment.

The importance of the entrainment of large droplets at low gas-flow velocities with respect to the enhancement of turbulence in the liquid boundary at the phase interface in the early state of steam-pocket formation could not be clarified completely. Sometimes relatively slow-moving disturbances of the steam–water interface or water droplets of the size of millimeters were observed in correspondence to steam velocities in the range of 20–40 m/s. This is in agreement with the experience from other entrainment processes with air and water for steady-state conditions (cf. Prandtl *et al.* 1969; Wallis 1969). According to figure 8b the steam pocket exists only for about 100 ms. During this time the steam velocity in the bottle-neck increases from 45 m/s up to some 100 m/s (cf. figure 8c). If we assume that the process of droplet formation in the case of smaller droplets is much faster than in the case of larger droplets, we conclude that with fast, increasing steam velocity the condensation effect of the finest droplets covers at last all other entrainment processes.

Comparison of our results with VCS experiments reported in the literature reveals, in terms of the phenomenology, that Aust & Sakkal (1981) also observed a pipe inner-annulus-type VCS. But in their experiment it was not possible to see that the annulus is connected to the steam column in the upper part of the condensation pipe for almost its total lifetime.

A similar assessment for the "bubble-type" VCS reveals a peak heat-transfer rate of roughly 120 MW/m^2, normalized for comparison with the vent-pipe cross-section area. Lee & Chan have reported such experiments with encapsulating steam bubbles (Lee 1979; Lee & Chan 1980; Lee 1983) which have almost the same steam mass flow rate as our experiments. They observed roughening of the two-phase interface at the lower part of the bubble in combination with turbulence within the liquid boundary layer. In comparison with our test results these roughening phenomena can clearly be identified to be consequences of the entrainment. In our films a liquid film is seen originating from the wetted pipe inner wall and trickling down from the pipe edge in the case of the encapsulating steam bubble (cf. figure 5b). Droplets of this film are thrust aside and atomized by the steam flow around the pipe edge and hit the bubble interface around the largest diameter of the bubble. The pipe itself became the bottle-neck where KHI is occurring at the wetted wall and therefore the main entrainment is starting. In comparison with the other VCS types the mass flow rate of entrained droplets must be reduced because of the relatively thin fluid film at the wetted pipe wall. The observed turbulence, which is assigned (Lee 1983) the responsibility for the enhanced heat transfer, results from these atomized droplets hitting the interface inside the steam pocket at a very high velocity.

To date the only effect known about a VCS was this roughening of the phase interface. So theoretical models, like the computer code KONDAS (Class 1977), manipulated the heat-transfer resistance in the boundary layer of the fluid, to model the transient increase of the heat-transfer

coefficient during a VCS. The manipulation was done, for example, by increasing the "renewing frequency" of the boundary layer, simulating the turbulent heat transfer in the fluid normal to the phase interface. This renewal frequency must be increased by about 2 orders of magnitude to simulate roughly a VCS. This complies with the data reported by Bankoff (1980) and those found here. A complete explanation of the VCS phenomenon however has to include the effect of direct steam condensation at the droplet surfaces.

7. CONCLUSIONS

In our experiments with a 30° sector of a PSS pool containing a 30° sector of a condensation pipe we found different VCS types which have been described, in part, previously by other authors. The transient heat-transfer coefficients deduced from our data are in accordance with those published in the literature (Catton *et al.* 1980; Lee 1983). However, in our work a better physical understanding of the highly transient phenomenon has been achieved. This was made possible by the special geometry of our experimental facility. Having a vertical cut through the phase interface, it revealed that the formation of a "steam pocket" with a "bottle-neck" is necessary to initiate a VCS.

The steam pockets, formed by the free interface of steam and water, have very different sizes and shapes. With the observation of self-amplifying strong entrainment and water atomization due to the steam flow through the bottle-neck of the steam pocket, which leads to a sharp increase in the heat-transfer coefficient and initiates a depressurization wave in the steam volume, the backfeed mechanism of a "steam-pocket instability" was identified which lasts until the steam pocket has disappeared. Due to the depressurization wave the entrainment and high condensation rates often propagate outside the steam pocket into the vent pipe.

REFERENCES

AUST, E. & SAKKAL, F. 1981 Review of GKSS 3-Vent experimental program and results. In *Proc. Int. Specialist Mtg on BWR-Pressure Suppression Containment Technology*, Geesthacht, F.R.G. (Edited by SCHULTHEISS, G. F.). Report GKSS 81/E/27.

BANKOFF, S. G. 1980 Some condensation studies pertinent to LWR safety. *Int. J. Multiphase Flow* **6,** 51–67.

BOURE, J. A., BERGLES, A. E. & TONG, L. S. 1973 Review of two-phase flow instability. *Nucl. Engng Des.* **25,** 165–192.

CATTON, I., CHAN, C. K., DHIR, V. K. & SIMPSON, M. 1980 Hydrodynamics of a vapor jet in subcooled liquid. Report NUREG/CR-1632.

CHAN, C. K. & LEE, C. K. B. 1982 A regime map for direct contact condensation. *Int. J. Multiphase Flow* **8,** 11–20.

CLASS, G. 1977 Theoretical investigation of pressure pulse development during steam condensation in the pressure reducing system of boiling water reactors—computer program KONDAS. Reports KfK 2487 (1977) and NUREG/TR-0028 R4 (1978).

CLASS, G. 1981 Multi-vent system problems. In *Proc. Int. Specialists Mtg on BWR-Pressure Suppression Containment Technology*, Geesthacht, F.R.G. (Edited by SCHULTHEISS, G. F.). Report GKSS 81/E/27.

CUMO, M., FARELLO, G. E. & FERRARI, G. 1978 Direct heat transfer in pressure-suppression systems. *6th Int. Heat Transfer Conf.*, Toronto, Paper NR-18.

LANGNER, H. 1978 Untersuchungen des Entrainment-Verhaltens in stationären und transienten zweiphasigen Ringströmungen. Dissertation, Technische Universität Hannover, Hannover, B.R.D.

LEE, C. K. B. 1979 Hydrodynamical aspects of low flow vapour injection into subcooled water. Ph.D. Dissertation, UCLA, Los Angeles, Calif.

LEE, C. K. B. & CHAN, C. K. 1980 An experimental study of low flow steam injection into subcooled water. In *Basic Mechanism in Two-phase Flow and Heat Transfer* (Edited by ROTHE, P. H. & LAHEY, R. T.). Presented at *ASME Winter Mtg*, Chicago, Ill.

LEE, C. K. B. 1983 Turbulent heat transfer on the surface of a steam-chugging bubble. *Int. Commun. Heat Mass Transfer* **10**, 25–37.

MARKS, J. S. & ANDEN, G. B. 1979 Chugging and condensation oscillation. In *Condensation Heat Transfer* (Edited by MARTO, P. J. & KRÖGER, P. G.). Presented at the *18th National Heat Transfer Conf.*, San Diego, Calif.

PRANDTL, L., OSWATITSCH, K. & WIEGHARDT, K. 1969 *Führer durch die Strömungslehre*. Vieweg, Braunschweig.

SONIN, A. A. 1981 Recent research at MIT on fluid–structure interactions, chugging, and scaling laws for SRV discharges. In *Proc. Int. Specialist Mtg on BWR-Pressure Suppression Containment Technology*, Geesthacht, F.R.G. (Edited by SCHULTHEISS, G. F.). Report GKSS 81/E/27.

WALLIS, G. B. 1969 *One-dimensional Two-phase Flow*. McGraw-Hill, New York.